Photochemical & Photobiological Sciences

RSC Publishing

PAPER

View Article Online
View Journal | View Issue

Cite this: *Photochem. Photobiol. Sci.*, 2013, **12**, 602

Brookite *versus* anatase TiO_2 photocatalysts: phase transformations and photocatalytic activities†

Tarek A. Kandiel,*[a,b] Lars Robben,[c] Ayad Alkaim[a,d] and Detlef Bahnemann*[a]

Received 26th June 2012,
Accepted 9th August 2012

DOI: 10.1039/c2pp25217a

www.rsc.org/pps

Titanium dioxide nanoparticles consisting of pure anatase, anatase-rich, brookite-rich, and pure brookite modifications were synthesized and characterized by X-ray diffraction, field emission-scanning electron microscopy and nitrogen adsorption. The phase transformations among the three modifications of TiO_2 (anatase, brookite, and rutile) and the photocatalytic activities of these nanoparticles were investigated by heat treatment over the temperature range from 400 to 800 °C and by the photooxidation of methanol, respectively. Direct transformation of anatase and brookite to rutile was observed, while in the case of the anatase–brookite mixture, anatase transforms firstly to brookite and then to rutile. The photocatalytic activity measurements indicate that brookite nanoparticles exhibit higher photocatalytic activities than anatase, and a comparable activity to that of the anatase-rich nanoparticles. The phase transformations and photocatalytic results are discussed regarding their dependence on crystallite size, surface area, and phase composition.

Introduction

Titanium dioxide (TiO_2) is an important material for various environmental and technical applications, *e.g.*, photocatalysis, dye-sensitized solar cells, photovoltaic and self-cleaning materials.[1–3] It exists commonly in nature in three phases: anatase, brookite and rutile. Under ambient conditions macrocrystalline rutile is thermodynamically stable relative to macrocrystalline anatase and brookite. However, the phase transitions between the three phases are dependent on many factors such as particle size, pH, surface energy, and solution chemistry.[4–8] For instance, if the particle sizes of the three phases are equal, anatase is the most thermodynamically stable phase for crystal sizes below *ca.* 11 nm, brookite is most stable for crystal sizes between *ca.* 11 and 35 nm, and rutile is most stable for crystal sizes exceeding 35 nm.[9]

Upon heating which is usually accompanied by a coarsening of the crystals, the crystal growth leads to alterations of phase stability and, ultimately, to the transformation of both, anatase and brookite, to rutile. The transformation of anatase to rutile is well studied and commonly observed.[5,10,11] However, it is unclear whether anatase transforms to brookite, or *vice versa*. Calorimetric data for the transformation enthalpies of anatase to rutile, and of brookite to rutile, suggest that the thermodynamic phase stability for the three polymorphs is rutile > brookite > anatase.[12] Accordingly, anatase may either transform directly to rutile, or initially to brookite and then to rutile. Ye *et al.*, however, reported that brookite transforms to anatase and then to rutile.[13] In contrast, Zhang and Banfield reported that anatase transforms to brookite and/or rutile before brookite transforms to rutile.[9]

Due to the thermodynamic stability of anatase nanoparticles with crystal sizes below *ca.* 11 nm relative to brookite and rutile and the ease of their synthesis, they are commonly employed in TiO_2 photocatalysis, however, it was reported that brookite nanocrystals exhibit markedly high photocatalytic activities as compared to those of rutile and anatase.[14–20] The difficulties encountered in brookite and tailored anatase/brookite nanoparticle preparation limit the information available about the thermal stability and the photocatalytic activities of anatase–brookite mixtures and of brookite TiO_2 nanoparticles in comparison with that of anatase nanoparticles.[21,22] Thus, further investigation of these materials is still of great importance. In the present paper, tailored anatase–brookite mixtures, and pure brookite TiO_2 nanoparticles were hydrothermally synthesized.[17] The phase transformation behavior of these materials at different temperatures (400 to 800 °C), as well as their photocatalytic activities toward methanol photooxidation, were investigated and discussed regarding their dependence on their crystallite size, surface area, and phase composition.

[a]*Institute of Technical Chemistry, Photocatalysis and Nanotechnology Research Unit, Leibniz Universität Hannover, Callinstr.3, 30167 Hannover, Germany. E-mail: bahnemann@iftc.uni-hannover.de; Fax: +49 511 762 2774; Tel: +49 511 762 5560*

[b]*Department of Chemistry, Faculty of Science, Sohag University, Sohag 82524, Egypt. E-mail: kandiel@iftc.uni-hannover.de*

[c]*Chemische Kristallographie fester Stoffe – FB2, Universität Bremen, Leobener Straße/NW2, D-28359 Bremen, Germany*

[d]*Department of Chemistry, College of Science, Babylon University, Hilla, Iraq*

†This paper is published as part of the themed issue of contributions from the 7th European Meeting on Solar Chemistry and Photocatalysis: Environmental Applications held in Porto, Portugal, June 2012.

Experimental

Preparation of TiO_2 nanoparticles

Pure anatase, anatase-rich, brookite-rich, and pure brookite TiO_2 nanoparticles were synthesized according to a previously reported method.[17] Briefly, 10 ml of titanium bis(ammonium lactate) dihydroxide (TALH) aqueous precursor (50%, Sigma-Aldrich) was added to 90 ml aqueous urea solution (0.1, 1.0, 2.0, and 6.0 M, respectively). The resulting solution was transferred to a Teflon cup and sealed in an autoclave and placed into an electric furnace held at 160 °C for 24 h. Then, the autoclave was naturally cooled in air. The resulting powders were separated by centrifugation, washed three times with water, and dried overnight at 60 °C in an oven. These materials were further calcined at different temperatures (400–800 °C) for 2 h in air.

Characterization of TiO_2 nanoparticles

XRD data for the Rietveld phase analysis of the TiO_2 nanoparticles were recorded on a Bruker AXS D4 Endeavour diffractometer using a reflection geometry with fixed divergence slits, $CuK\alpha_{1,2}$ radiation, and a Nickel filter. Three thousand data points were collected with a step width of 0.02° and 2 s measurement times per step in the 2θ range from 20 to 80°. The phase analysis by the Rietveld method was carried out using the TOPAS (Bruker AXS) software. During the refinements, general parameters such as scale factors, one background parameter, and the zero point error were optimized. Profile shape calculations were carried out on the basis of standard instrumental parameters using the fundamental parameter approach implemented in the program, varying also the average crystal size (integral breadth) of the reflections. Lattice parameters and crystallite size of all phases were refined. Structural data for anatase, rutile, and brookite phases were taken from ICSD database (anatase [9854], rutile [62 679], and brookite [36 410]).

Field emission-scanning electron microscope (FE-SEM) measurements were carried out on a JEOL JSM-6700F field emission instrument using a secondary electron detector (SE) at an accelerating voltage of 2 kV.

Single-point standard BET surface area measurements were carried out employing a Micromeritics AutoMate 23 instrument. The gas mixture used for the adsorption determinations was 30% nitrogen and 70% helium.

Photocatalytic activity measurement

The methanol photooxidation reaction was studied employing a water cooled double jacket quartz photoreactor at 25 °C. 0.065 g of TiO_2 nanoparticles were suspended in 65 ml of 30 mM aqueous methanol solution by sonication. Then, the suspension was transferred to the photoreactor and stirred in the dark for 30 min to reach the adsorption equilibrium with molecular oxygen being purged through the reaction vessel continuously. The photoreactor was irradiated from the outside using an Osram XBO 450 W Xenon lamp in a Müller LAX 1000 lamp housing. The lamp was switched on 30 min prior to the start of the reaction to stabilize the power of its emission at $\lambda > 320$ nm (a cut off filter was used to remove light with wavelengths below 320 nm). Samples were withdrawn at regular intervals from the upper part of the reactor with the catalyst being removed from the liquid phase by filtration through nylon syringe filters (pore size: 0.45 μm). The photooxidation rate was determined by measuring the HCHO generated as a result of the methanol oxidation during the first 60 min of illumination employing the Nash method. This method is based on the reaction of formaldehyde with acetylacetone and ammonium acetate to form a yellow colored product with a maximum of absorbance at 412 nm. Measurements were carried out using a Varian Cary 100 Scan UV-vis spectrophotometer, following an incubation time of 15 min at 60 °C.

Results and discussion

Phase transformations

The Rietveld refinements of the XRD patterns of the as-prepared TiO_2 nanoparticles presented in Fig. 1(a) indicate that the pure anatase (A), anatase-rich (AB, *ca.* 82 wt% anatase with the rest being brookite), brookite-rich (BA, *ca.* 77 wt% brookite with the rest being anatase), and pure brookite (B) TiO_2 nanoparticles were obtained in the presence of 0.1, 1.0, 2.0, and 6.0 M urea, respectively. Fig. 1(b) and (c) shows the XRD patterns of anatase and brookite calcined at different temperatures, respectively. It is readily discernible from the diffraction peak located at 27.45° (2θ) in the XRD pattern in Fig. 1(b) that anatase is partially transformed to rutile upon calcination at 600 °C. Upon further increase of calcination temperatures, the weight percentage of rutile increases at the expense of anatase, while no brookite is formed as evinced by the Rietveld analysis (see Table 1). This direct transformation of anatase to rutile is commonly reported and is assumed to take place *via* interfacial nucleation at certain contact areas between two anatase particles.[10,11]

The XRD patterns presented in Fig. 2(c) clearly show that brookite nanoparticles are thermally stable up to 700 °C, as can be seen from the (121) diffraction peak located at 30.81° (2θ) where no overlapping of this reflection with any peak from anatase or rutile occurs. The XRD pattern obtained at 800 °C indicates that brookite is directly transformed to rutile as it is readily discernible from the (110) diffraction peak of rutile located at 27.45° (2θ). No reflections related to anatase were detected. The latter observation could be explained by the fact that the transformation sequence amongst anatase, brookite, and rutile is size dependent, because the energies of the three polymorphs are sufficiently close that they can be reversed by small differences in surface energy. As mentioned in the introduction section, anatase is most thermodynamically stable at crystallite sizes below 11 nm, brookite is most stable for crystal sizes between 11 and 35 nm, and rutile is most stable at sizes exceeding 35 nm.[9] The as-prepared brookite nanoparticles employed in this study have crystallite size of 38 nm as observed from the Rietveld refinements of the XRD patterns (see Table 1). Particle coarsening upon heat treatment leads to

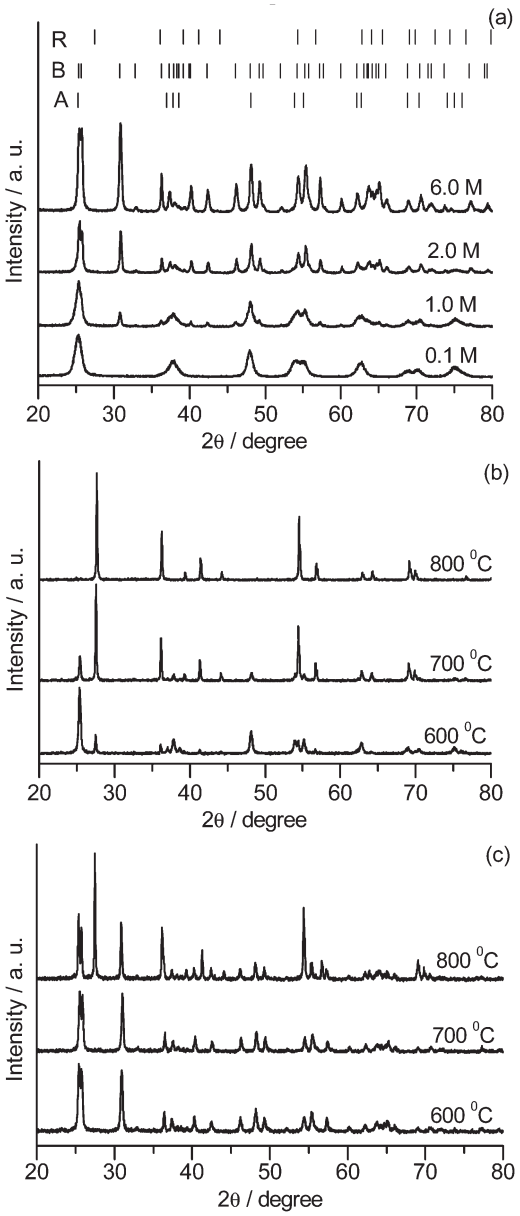

Fig. 1 XRD patterns of (a) TiO_2 nanoparticles prepared in the presence of different urea concentrations, (b) as-prepared anatase, and (c) as-prepared brookite TiO_2 nanoparticles calcined at different temperatures for 2 h in air. A, B, and R indicate the Bragg positions for anatase, brookite, and rutile, respectively.

an increase of the crystallite size up to 41 nm at 700 °C. At higher temperatures (800 °C), the crystallite size becomes bigger and simultaneously the brookite phase is transformed to rutile, the most stable phase under these conditions. By comparison of the phase transformations of anatase to rutile and of brookite to rutile presented in Fig. 1(b) and (c), respectively, it can be concluded that anatase nanoparticles are transformed faster to rutile than brookite, *e.g.*, at 700 °C after 2 h 79 wt% of anatase is already transformed to rutile while brookite is still stable. The faster transformation of anatase nanoparticles to rutile is attributed to their smaller crystallite size, *i.e.*, 6 nm (see Table 1), and to their aggregate state. In general, the transformation rate among different TiO_2 phases depends on the particle size and on the aggregation state. For instance, it was reported that the transformation rate of anatase to rutile is increased dramatically when the reacting anatase is very finely crystalline and aggregated due to increased contact sites between the nanoparticles which are suggested to be the potential nucleation sites.[6,23]

Fig. 2(a) and (b) shows the XRD patterns of the anatase-rich (AB) and brookite-rich (BA) TiO_2 particles calcined at different temperatures, respectively. The phase composition and the crystallite size obtained from the Rietveld refinements of these XRD patterns are given in Table 1. It can be clearly seen from the data presented in Table 1, that in the case of the anatase–brookite mixtures, anatase is transformed to brookite first, after which both of them are transformed to rutile. For example, in the case of AB nanoparticles, the brookite content in the as-prepared sample increases from 18 wt% to 32 wt% at 600 °C, while the anatase content decreases from 82 wt% to 67 wt% at the corresponding calcination temperature. Interestingly, in the case of brookite-rich nanoparticles, the content of brookite in the as-prepared sample increases from 77 wt% to 100% at 600 °C, enabling the preparation of highly crystalline brookite, free of any anatase. At higher temperatures (*i.e.*, exceeding or equal to 700 °C), the crystallite sizes of anatase and brookite are increasing significantly, before they are transformed to rutile, which is the thermodynamically more stable phase in the bigger crystallite size range. The transformation of anatase to brookite can be explained by the fact that under the present conditions brookite exhibits a higher thermal stability than anatase and thus brookite particles can act as nucleation sites for the anatase to brookite transformation.

To analyze the morphology change after the calcination, some selected samples were investigated by field emission-scanning electron microscopy (SEM). Fig. 3(a) and (b) shows the SEM micrographs of anatase TiO_2, as-prepared and after calcination at 800 °C for 2 h, respectively. It can be clearly seen from micrograph (a) that the as-prepared anatase TiO_2 aggregates form very fine particles in the size range of *ca.* 10 nm or even less. After calcination, the particle sizes increase from *ca.* 10 nm to *ca.* 100 nm and the shape of the particles transforms from sphere-like to irregular shape as shown in micrograph (b). Fig. 3(c) and (d) show the SEM micrographs of the as-prepared brookite TiO_2 nanoparticles and of the same particles after calcination at 700 °C for 2 h, respectively. Micrograph (c) evinces that brookite consists of rods with diameters up to 25 nm and lengths up to 150 nm. After calcination, the rod like particles can still be clearly seen but their diameters are bigger while their lengths are reduced (see micrograph d). Fig. 3(e) and (f) shows the SEM micrographs of anatase-rich and brookite-rich TiO_2 nanoparticles calcined at 700 °C and at 600 °C for 2 h, respectively. Micrograph (e) indicates the anatase-rich TiO_2 aggregates of particles in the size range of *ca.* 50 nm, while micrograph (f) shows the brookite-rich TiO_2 aggregates of rod-like particles with diameters up to 50 nm and lengths up to 100 nm.

Table 1 Textural properties of anatase (A), anatase-rich (AB), brookite-rich (BA), and brookite (B) TiO_2 nanoparticle powders calcined at different temperatures

TiO_2 nanoparticles	Temperature/°C	$S_{BET}/m^2\ g^{-1}$	Anatase/wt%	Crystallite size/nm	Rutile/wt%	Crystallite size/nm	Brookite/wt%	Crystallite size/nm
Anatase	a.p.	151	100	6				
	600	2.1	84	34	16	82		
	700	1.2	21	42	79	104		
	800	0.8			100	124		
Anatase-rich	a.p.	139	82	7			18	19
	400	100	80	10			20	22
	600	31	67	24			32	66
	700	14	66	49	6	45	28	74
	750	12	47	58	49	61	5	12
	800	1.5	5	46	95	73		
Brookite-rich	a.p.	64	23	6			77	34
	400	49	22	7			78	41
	600	25					100	50
	700	16			5	60	95	60
	750	13			60	111	40	52
	800	9			96	145	4	47
Brookite	a.p.	53					100	38
	600	31					100	39
	700	26					100	41
	800	14			45	126	55	65

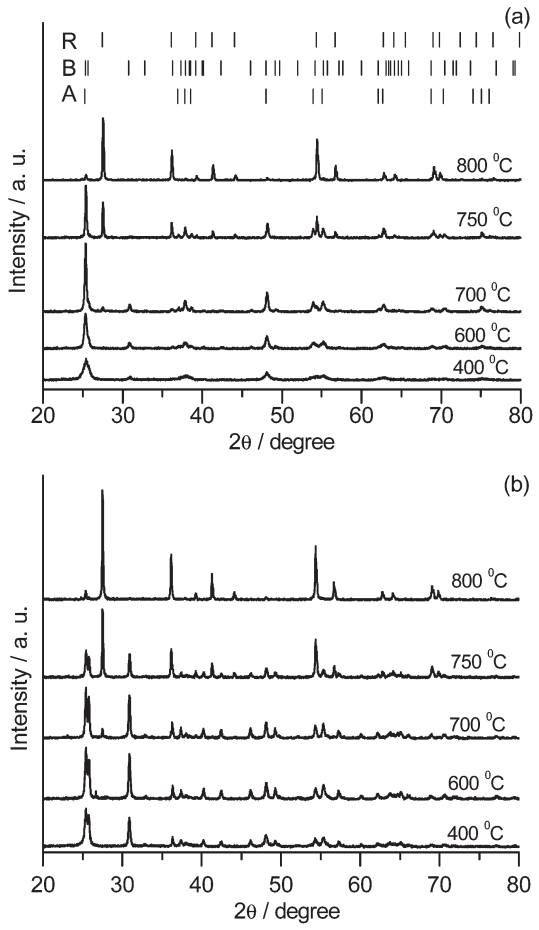

Fig. 2 XRD patterns of anatase-rich (a) and brookite-rich (b) TiO_2 nanoparticles calcined at different temperatures for 2 h in air. A, B, and R indicate the Bragg positions for anatase, brookite, and rutile, respectively.

Photocatalytic activities

The photocatalytic activities of the as-prepared and the calcined TiO_2 nanoparticles were assessed by determining the photonic efficiencies of methanol photooxidation. When TiO_2 absorbs a photon, the energy of which exceeds its bandgap energy, an electron (e^-)/hole (h^+) pair is generated. Both e^- and h^+ can either migrate to the TiO_2 surface and react with adsorbed reactants in a photocatalytic process or may undergo an undesired recombination. In the presence of molecular O_2 and methanol, the excited electron reacts with the former leading to the formation of the superoxide radical ($O_2^{-\cdot}$) while the latter reacts with the hole either directly through a trapped hole or indirectly through a surface hydroxyl radical $OH^{\cdot}$ as intermediate leading to the formation of $^{\cdot}CH_2OH$. The $^{\cdot}CH_2OH$ radical further reacts with molecular oxygen leading to the formation of formaldehyde (HCHO) as the first stable intermediate (which will subsequently be further oxidized yielding carbon dioxide as the final product).[24–26] Fig. 4(a) and (b) shows some examples of the time course of the formaldehyde formation upon irradiation on TiO_2 nanoparticles as-prepared (a) and after calcination at 600 °C for 2 h (b). The photonic efficiencies (ξ) of the methanol photooxidation were calculated by dividing the rate of formaldehyde formation by the photon flux according to eqn (1).[27,28] The rate of formaldehyde formation (r) was calculated from the slope of Fig. 4. The incident photon flux (I_0) per volumetric unit was calculated according to eqn (2) to be 7.63×10^{-3} einstein $l^{-1}\ h^{-1}$ assuming an average illumination wavelength $\lambda = 350$ nm.

$$\xi = \frac{r}{I_0} \times 100 \quad (1)$$

$$I_0 = \frac{I\lambda A}{N_A hcV} \quad (2)$$

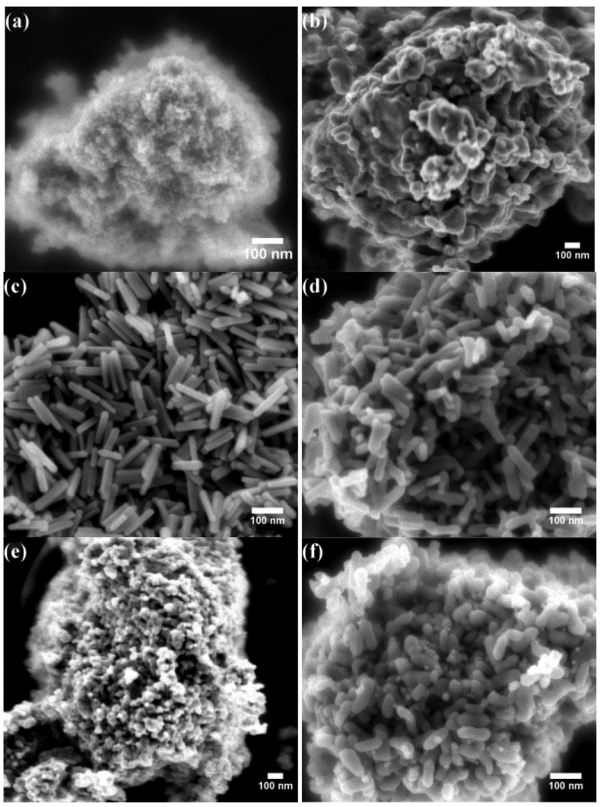

Fig. 3 SEM micrographs of TiO_2 nanoparticles (a) as-prepared anatase, (b) anatase calcined at 800 °C, (c) as-prepared brookite, (d) brookite calcined at 700 °C, (e) anatase-rich calcined at 700 °C, and (f) brookite-rich calcined at 600 °C.

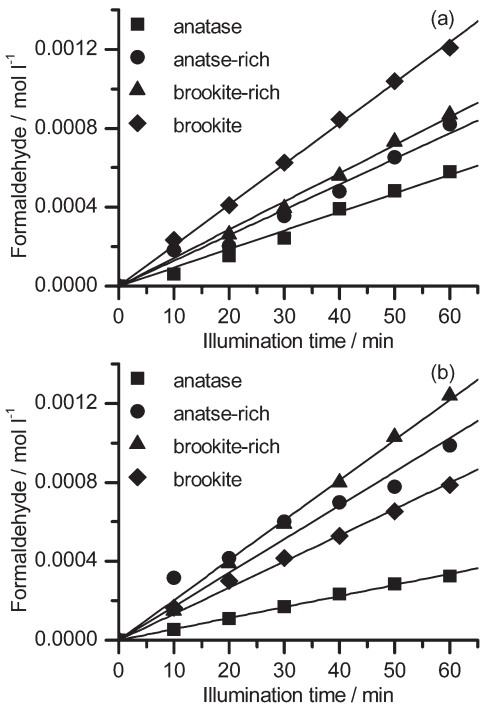

Fig. 4 Time course of formaldehyde formation on TiO_2 nanoparticles (a) as-prepared and (b) calcined at 600 °C for 2 h.

The irradiated surface area (A) was 3.14 cm^2; the light intensity (I) based upon UV-A light meter measurements was *ca.* 15 J s^{-1} cm^{-2}; the volume of the employed suspension (V) was 0.065 l, N_A (Avogadro's number) = 6.02×10^{23} mol^{-1}, h (Planck's constant) = 6.63×10^{-34} J s, c (light velocity) = 2.99×10^8 m s^{-1}.

Under the present experimental conditions, the inner part of the employed photoreactor is long enough (*ca.* 5 cm) to ensure that no light is transmitted and, therefore, the incident light is completely absorbed by the TiO_2 suspensions, except for the fraction of light that is backscattered. Depending on the diffuse reflectance measurements (data not shown), it is reasonable to assume that the fraction of the backscattered light is almost identical for all photocatalysts investigated here. Thus, the photonic efficiencies were calculated assuming the investigated powders absorb the same amount of light. The calculated photonic efficiencies of the photocatalytic formaldehyde formation on anatase (A), anatase-rich (AB), brookite-rich (BA), and brookite (B) TiO_2 nanoparticles, as-prepared and calcined at different temperatures, are presented in Fig. 5. For comparison the photonic efficiency measured with TiO_2 P25 (Evonik-Degussa Airoxide) as the photocatalyst is also presented.

It can be seen from Fig. 5(a) and (c) that the as-prepared TiO_2 anatase nanoparticles (A-a.p) exhibit two times lower photonic efficiency than the as-prepared brookite nanoparticles (B-a.p.) despite the fact that the surface area of the former is *ca.* three times higher than that of the latter (see Table 1). This higher activity of brookite nanoparticles can be attributed to their higher crystallinity, *e.g.*, the crystallite size of brookite nanoparticles is *ca.* 25 nm, while the crystallite size of the anatase nanoparticles is *ca.* 4 nm (see Table 1), and/or to the cathodic shift of the conduction band of brookite

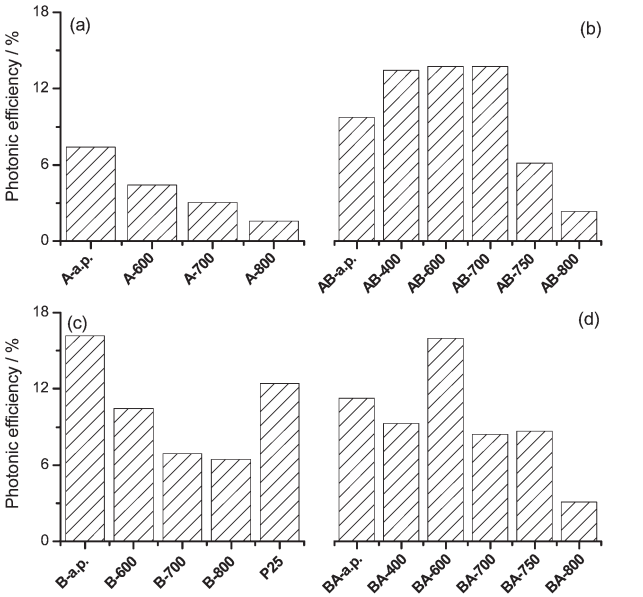

Fig. 5 Photonic efficiencies of formaldehyde formation on (a) anatase, (b) anatase-rich, (c) brookite, and (d) brookite-rich TiO_2 nanoparticles, as-prepared and calcined at different temperatures, from 30 mM methanol aqueous suspensions upon illumination.

nanoparticles as compared with that of anatase nanoparticles as previously reported.[17,29] This shift should facilitate the interfacial electron transfer to molecular oxygen and thus accelerate the overall photocatalytic process. However, at this point it is worth mentioning that the photocatalytic activity depends on many factors, *e.g.*, on surface area, crystallinity, phase composition, bandgap energy, conduction band level, test reaction, as well as on many other properties. Thus, a direct dependency between the physical properties of a photocatalyst and its photocatalytic activity is a complex matter and it is usually not easy to conclude a direct correlation which is valid for all photocatalysts prepared under different conditions.[21,30,31]

The calcination of anatase or brookite nanoparticles leads to a decrease of the surface area, to an increase of the crystallinity, and to the formation of the rutile phase (see Table 1). The continuous decrease of the photocatalytic activities of anatase and brookite nanoparticles upon calcination, in fact, correlates well with the decrease of the surface area, and thus, it can be attributed to the decrease of the surface area and/or to the formation of rutile, being the less active phase. However, since the crystallinity is enhanced after calcination, the decrease of the photocatalytic activity supports the fact that the methanol photooxidation is dominated by the particle's surface area rather than by its crystallinity. By comparing the photonic efficiencies of anatase-rich and brookite-rich nanoparticles calcined at different temperatures presented in Fig. 5(b) and (d), respectively, with that of anatase and brookite nanoparticles calcined at the relevant temperatures presented in Fig. 5 (a) and (c), respectively, it can be seen that, in general, the former exhibit higher photocatalytic activities than anatase nanoparticles and a comparable or even higher activity than that of brookite, except for the as-prepared brookite nanoparticles. The higher activity of the anatase-rich particles can be explained by a synergistic effect between anatase and brookite nanoparticles. The conduction band edge of TiO_2 brookite has been found to be about 0.14 eV more negative than that of anatase.[17] This readily suggests a facilitated interfacial electron transfer, and the energy barrier will suppress the back electron transfer. Consequently, the holes left in the valence band of brookite efficiently oxidize methanol, while the electrons having moved to the anatase are consumed by the reduction of molecular oxygen. This will lead to a better charge carrier separation and thus to an increase of the photocatalytic activity. An analogous synergistic effect is also commonly observed between anatase and rutile phases[32–35] and is moreover experimentally supported by photodeposition experiments of Ag.[36] However, in the case of brookite-rich nanoparticles, this synergistic effect has not been observed before, as pure brookite showed higher photocatalytic activity than the brookite-rich nanoparticles (see Fig. 5(c) and (d)).

Conclusions

As-prepared anatase (crystallite size 6 nm) and brookite (crystallite size *ca.* 38 nm) TiO_2 nanoparticles transform directly to rutile upon calcination under air. The latter show thermal stability up to 700 °C while the former start to transform to rutile at 600 °C. A higher transformation rate of anatase to rutile, as compared with that of brookite to rutile, is observed and explained by increased contact sites between the anatase nanoparticles, resulting from their aggregation, which act as sites for the rutile nucleation. In the case of anatase-rich or brookite-rich nanoparticles, anatase transforms to brookite at temperatures below or equal to 600 °C due to the thermodynamic stability of brookite under these conditions (crystallite sizes *ca.* 19 nm up to 50 nm). At higher temperatures, *i.e.*, exceeding or equal to 700 °C, both anatase and brookite are transformed to rutile. The photocatalytic activity measurements indicate that brookite nanoparticles exhibit higher activity toward methanol photooxidation than anatase nanoparticles. This difference is explained by considering the crystallinity and the conduction band position of both phases. The higher photocatalytic activity of the anatase-rich nanoparticles compared with that of anatase nanoparticles is explained by a synergistic effect between anatase and brookite. Pure brookite nanoparticles exhibit a higher photocatalytic activity than brookite-rich nanoparticles.

Acknowledgements

Financial support from the Bundesministerium für Bildung und Forschung (BMBF) is gratefully acknowledged (grant no. 01RC1012C). T. A. Kandiel thanks the Chemistry Department, Faculty of Science, Sohag University for granting him a leave of absence.

Notes and references

1 M. R. Hoffmann, S. T. Martin, W. Y. Choi and D. W. Bahnemann, Environmental applications of semiconductor photocatalysis, *Chem. Rev.*, 1995, **95**, 69–96.
2 K. Hashimoto, H. Irie and A. Fujishima, TiO_2 photocatalysis: a historical overview and future prospects, *Jpn. J. Appl. Phys.*, 2005, **44**, 8269–8285.
3 M. Gratzel, Dye-sensitized solar cells, *J. Photochem. Photobiol., C*, 2003, **4**, 145–153.
4 A. A. Gribb and J. F. Banfield, Particle size effects on transformation kinetics and phase stability in nanocrystalline TiO_2, *Am. Mineral.*, 1997, **82**, 717–728.
5 H. Z. Zhang and J. F. Banfield, Thermodynamic analysis of phase stability of nanocrystalline titania, *J. Mater. Chem.*, 1998, **8**, 2073–2076.
6 M. P. Finnegan, H. Z. Zhang and J. F. Banfield, Phase stability and transformation in titania nanoparticles in aqueous solutions dominated by surface energy, *J. Phys. Chem. C*, 2007, **111**, 1962–1968.
7 M. P. Finnegan, H. Z. Zhang and J. F. Banfield, Anatase coarsening kinetics under hydrothermal conditions as a

function of pH and temperature, *Chem. Mater.*, 2008, **20**, 3443–3449.

8 T. A. Kandiel, R. Dillert and D. Bahnemann, Titanium dioxide nanoparticles and nanostructures, *Curr. Inorg. Chem.*, 2012, **2**, 94–114.

9 H. Z. Zhang and J. F. Banfield, Understanding polymorphic phase transformation behavior during growth of nanocrystalline aggregates: insights from TiO_2, *J. Phys. Chem. B*, 2000, **104**, 3481–3487.

10 H. Z. Zhang and J. F. Banfield, New kinetic model for the nanocrystalline anatase-to-rutile transformation revealing rate dependence on number of particles, *Am. Mineral.*, 1999, **84**, 528–535.

11 H. Z. Zhang and J. F. Banfield, Phase transformation of nanocrystalline anatase-to-rutile *via* combined interface and surface nucleation, *J. Mater. Res.*, 2000, **15**, 437–448.

12 M. R. Ranade, A. Navrotsky, H. Z. Zhang, J. F. Banfield, S. H. Elder, A. Zaban, P. H. Borse, S. K. Kulkarni, G. S. Doran and H. J. Whitfield, Energetics of nanocrystalline TiO_2, *Proc. Natl. Acad. Sci. U. S. A.*, 2002, **99**, 6476–6481.

13 X. S. Ye, J. Sha, Z. K. Jiao and L. D. Zhang, Thermoanalytical characteristic of nanocrystalline brookite-based titanium dioxide, *Nanostruct. Mater.*, 1997, **8**, 919–927.

14 B. Ohtani, J. Handa, S. Nishimoto and T. Kagiya, Highly-active semiconductor photocatalyst – extra-fine crystallite of brookite TiO_2 for redox reaction in aqueous propan-2-ol and or silver sulfate-solution, *Chem. Phys. Lett.*, 1985, **120**, 292–294.

15 N. Murakami, T. Kamai, T. Tsubota and T. Ohno, Novel hydrothermal preparation of pure brookite-type titanium (IV) oxide nanocrystal under strong acidic conditions, *Catal. Commun.*, 2009, **10**, 963–966.

16 A. A. Ismail, T. A. Kandiel and D. W. Bahnemann, Novel (and better?) titania-based photocatalysts: brookite nanorods and mesoporous structures, *J. Photochem. Photobiol., A*, 2010, **216**, 183–193.

17 T. A. Kandiel, A. Feldhoff, L. Robben, R. Dillert and D. W. Bahnemann, Tailored titanium dioxide nanomaterials: anatase nanoparticles and brookite nanorods as highly active photocatalysts, *Chem. Mater.*, 2010, **22**, 2050–2060.

18 M. Addamo, M. Bellardita, A. Di Paola and L. Palmisano, Preparation and photoactivity of nanostructured anatase, rutile and brookite TiO_2 thin films, *Chem. Commun.*, 2006, 4943–4945.

19 V. Augugliaro, V. Loddo, M. J. Lopez-Munoz, C. Marquez-Alvarez, G. Palmisano, L. Palmisano and S. Yurdakal, Home-prepared anatase, rutile, and brookite TiO_2 for selective photocatalytic oxidation of 4-methoxybenzyl alcohol in water: reactivity and ATR-FTIR study, *Photochem. Photobiol. Sci.*, 2009, **8**, 663–669.

20 L. J. Zhang, V. M. Menendez-Flores, N. Murakami and T. Ohno, Improvement of photocatalytic activity of brookite titanium dioxide nanorods by surface modification using chemical etching, *Appl. Surf. Sci.*, 2012, **258**, 5803–5809.

21 H. Kominami, Y. Ishii, M. Kohno, S. Konishi, Y. Kera and B. Ohtani, Nanocrystalline brookite-type titanium(IV) oxide photocatalysts prepared by a solvothermal method: correlation between their physical properties and photocatalytic activities, *Catal. Lett.*, 2003, **91**, 41–47.

22 S. Bakardjieva, V. Stengl, L. Szatmary, J. Subrt, J. Lukac, N. Murafa, D. Niznansky, K. Cizek, J. Jirkovsky and N. Petrova, Transformation of brookite-type TiO_2 nanocrystals to rutile: correlation between microstructure and photoactivity, *J. Mater. Chem.*, 2006, **16**, 1709–1716.

23 H. Zhang and J. F. Banfield, Size dependence of the kinetic rate constant for phase transformation in TiO_2 nanoparticles, *Chem. Mater.*, 2005, **17**, 3421–3425.

24 L. Z. Sun and J. R. Bolton, Determination of the quantum yield for the photochemical generation of hydroxyl radicals in TiO_2 suspensions, *J. Phys. Chem.*, 1996, **100**, 4127–4134.

25 J. R. Chuan-yi Wang, D. W. Bahnemann and J. K. Dohrmann, Photonic efficiency and quantum yield of formaldehyde formation from methanol in the presence of various TiO_2 photocatalysts, *J. Photochem. Photobiol., A*, 2002, **148**, 169–176.

26 T. A. Kandiel, R. Dillert and D. W. Bahnemann, Enhanced photocatalytic production of molecular hydrogen on TiO_2 modified with Pt-polypyrrole nanocomposites, *Photochem. Photobiol. Sci.*, 2009, **8**, 683–690.

27 N. Serpone and A. Salinaro, Terminology, relative photonic efficiencies and quantum yields in heterogeneous photocatalysis. Part I: suggested protocol (technical report), *Pure Appl. Chem.*, 1999, **71**, 303–320.

28 A. Salinaro, A. V. Emeline, J. C. Zhao, H. Hidaka, V. K. Ryabchuk and N. Serpone, Terminology, relative photonic efficiencies and quantum yields in heterogeneous photocatalysis. Part II: experimental determination of quantum yields (technical report), *Pure Appl. Chem.*, 1999, **71**, 321–335.

29 P. A. Di, M. Bellardita, R. Ceccato, L. Palmisano and F. Parrino, Highly active photocatalytic TiO_2 powders obtained by thermohydrolysis of $TiCl_4$ in water, *J. Phys. Chem. C*, 2009, **113**, 15166–15174.

30 S. Nishimoto, B. Ohtani, H. Kajiwara and T. Kagiya, Correlation of the crystal-structure of titanium-dioxide prepared from titanium tetra-2-propoxide with the photocatalytic activity for redox reactions in aqueous propan-2-ol and silver salt-solutions, *J. Chem. Soc., Faraday Trans. 1*, 1985, **81**, 61–68.

31 O. O. Prieto-Mahaney, N. Murakami, R. Abe and B. Ohtani, Correlation between photocatalytic activities and structural and physical properties of titanium(IV) oxide powders, *Chem. Lett.*, 2009, **38**, 238–239.

32 T. Ohno, K. Tokieda, S. Higashida and M. Matsumura, Synergism between rutile and anatase TiO_2 particles in photocatalytic oxidation of naphthalene, *Appl. Catal., A*, 2003, **244**, 383–391.

33 A. Zachariah, K. V. Baiju, S. Shukla, K. S. Deepa, J. James and K. G. K. Warrier, Synergistic effect in photocatalysis as observed for mixed-phase nanocrystalline titania processed *via* sol–gel solvent mixing and calcination, *J. Phys. Chem. C*, 2008, **112**, 11345–11356.

34 Y. K. Kho, A. Iwase, W. Y. Teoh, L. Madler, A. Kudo and R. Amal, Photocatalytic H-2 evolution over TiO_2 nanoparticles. The synergistic effect of anatase and rutile, *J. Phys. Chem. C*, 2010, **114**, 2821–2829.

35 T. A. Kandiel, R. Dillert, A. Feldhoff and D. W. Bahnemann, Direct synthesis of photocatalytically active rutile TiO_2 nanorods partly decorated with anatase nanoparticles, *J. Phys. Chem. C*, 2010, **114**, 4909–4915.

36 T. Kawahara, Y. Konishi, H. Tada, N. Tohge, J. Nishii and S. Ito, A patterned TiO_2(anatase)/TiO_2(rutile) bilayer-type photocatalyst: effect of the anatase/rutile junction on the photocatalytic activity, *Angew. Chem., Int. Ed.*, 2002, **41**, 2811–2813.